Characterization of Purified New Delhi Metallo-β-lactamase-1

ARTICLE *in* BIOCHEMISTRY · NOVEMBER 2011

Impact Factor: 3.02 · DOI: 10.1021/bi201449r · Source: PubMed

7 AUTHORS, INCLUDING:

Pei W Thomas
University of Texas at Austin
26 PUBLICATIONS **784** CITATIONS
SEE PROFILE

Shanshan Wu
University of California, San Francisco
9 PUBLICATIONS **129** CITATIONS
SEE PROFILE

Hua Guo
University of New Mexico
382 PUBLICATIONS **7,530** CITATIONS
SEE PROFILE

Dali Liu
Loyola University Chicago
32 PUBLICATIONS **433** CITATIONS
SEE PROFILE

BIOCHEMISTRY
including biophysical chemistry & molecular biology

Article

pubs.acs.org/biochemistry

Characterization of Purified New Delhi Metallo-β-lactamase-1

Pei W. Thomas,[†] Min Zheng,[‡] Shanshan Wu,[‡] Hua Guo,[§] Dali Liu,*[,∥] Dingguo Xu,*[,‡] and Walter Fast*[,†]

[†]Division of Medicinal Chemistry, College of Pharmacy, The University of Texas, Austin, Texas 78712, United States

[‡]Key Laboratory of Green Chemistry and Technology, Ministry of Education, College of Chemistry, Sichuan University, Chengdu, Schuan 610064, China

[§]Department of Chemistry and Chemical Biology, University of New Mexico, Albuquerque, New Mexico 87131, United States

[∥]Department of Chemistry, Bioinformatics Program, Loyola University Chicago, Chicago, Illinois 60660, United States

Supporting Information

ABSTRACT: New Delhi metallo-β-lactmase-1 (NDM-1) has recently emerged as a global threat because of its ability to confer resistance to almost all clinically used β-lactam antibiotics, its presence within an easily transmissible plasmid bearing a number of other antibiotic resistance determinants, its carriage in a variety of enterobacteria, and its presence in both nosocomial and community-acquired infections. To improve our understanding of the molecular basis of this threat, NDM-1 was purified and characterized. Recombinant NDM-1 bearing its native leader sequence was expressed in *Escherichia coli* BL21 cells. The major processed form found to be released into culture media contains a 35-residue truncation at the N-terminus. This form of NDM-1 is monomeric and can be purified with 1.8 or 1.0 equiv of zinc ion, depending on the experimental conditions. Treatment of dizinc NDM-1 with EDTA results in complete removal of both zinc ions, but the relatively weaker chelator PAR chelates only 1 equiv of zinc ion from folded protein but 1.9 equiv of zinc ion from denatured protein, indicating different affinities for each metal binding site. UV−vis spectroscopy of the dicobalt metalloform along with molecular dynamics simulations of the dizinc metallo form indicates that the dinuclear metal cluster at the active site of NDM-1 is similar in structure to other class B1 metallo-β-lactamases. Supplementation of excess zinc ions to monozinc NDM-1 has differential effects on enzyme activity with respect to three different classes of β-lactam substrates tested, penems, cephems, and carbapenems, and likely reflects dissimilar contributions of the second equivalent of metal ion to the catalysis of the hydrolysis of these substrates. Fits to these concentration dependencies are used to approximate the K_d value of the more weakly bound zinc ion (2 μM). NDM-1 achieved maximal activity with all substrates tested when supplemented with approximately 10 μM $ZnSO_4$, displaying k_{cat}/K_M values ranging from 1.4×10^6 to 2.0×10^7 M^{-1} s^{-1}, and a slight preference for cephem substrates. This work provides a foundation for an improved understanding of the molecular basis of NDM-1-mediated antibiotic resistance and should allow more quantitative studies to develop targeted therapeutics.

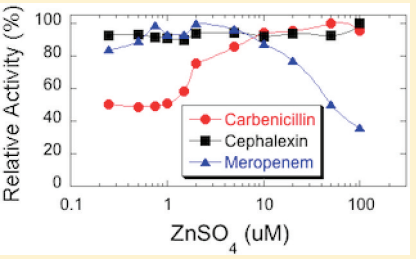

It is difficult to overstate the importance of β-lactam drugs for treating bacterial infections. Since shortly after their discovery and development, a number of different resistance mechanisms, including β-lactamases, have emerged.[1] One of the most troubling is the class B β-lactamase, also called metallo-β-lactamase (MBL). This class of lactamase is unlike the others in that its members do not use a covalent catalytic mechanism, thereby making it resistant to most lactam-based inhibitors.[2] Instead, hydrolysis of almost all clinically used β-lactams is catalyzed by one or two zinc ions at the active site of these enzymes.[3] The MBL family is very diverse, sharing less than 20% sequence identity between subclasses,[4] which carry different numbers of equivalents of zinc ions and use differing mechanisms. For example, subclass B1 metallo-β-lactamases use either 1 or 2 equiv of zinc. Subclass B2 enzymes use 1 equiv of zinc, but it is bound at a different site than in the monozinc B1 enzymes. Subclass B3 enzymes are generally binuclear zinc enzymes, but their primary metal ion coordination shell is divergent from those of the other subclasses.[3,5] Adjacent to their metal centers, each of these subclasses also has substrate-binding loops that vary significantly in placement, length, and sequence.[6−10]

The first MBL discovered was chromosomally encoded by the relatively innocuous *Bacillus cereus* microbe and was considered more of a biochemical curiosity than a clinical concern.[5,11] Since then, MBLs have grown into a looming global antibiotic resistance threat, most recently highlighted by the spread of a new NDM-1 "superbug", which is controversially[12] named after its most troubling antibiotic resistance determinant, New Delhi metallo-β-lactamase-1.[13] NDM-1 bearing *Klebsiella pneumoniae* and *Escherichia coli* infections, which were resistant to all β-lactams tested, were first discovered in India in 2008,[13] and NDM-1 infections have since rapidly spread to five of seven continents.[14] Some of the most troubling features are that NDM-1 is plasmid-borne, allowing rapid dissemination, and that this plasmid also carries

Received: September 17, 2011
Revised: October 26, 2011
Published: October 26, 2011

resistance determinants for macrolides, aminoglycosides, rifampicin, sulfamethoxazole, and monobactams.[14] Even more worrying are reports that NDM-1 infections may be acquired from community water supplies and not just from clinical settings.[15]

Despite its clinical importance, there have not yet been many studies that characterize the purified NDM-1 enzyme. At present, four reports of NDM-1 structural determinations have been published,[16−19] with additional coordinates available in the Protein Data Bank (PDB). These structural models show that NDM-1 has a typical MBL fold, but considerable differences exist between the models, including differences in the stoichiometry and identity of bound metal ions, the conformations of the coordinating ligands, the length of the N-terminus (which can impact the structure of the active site), and the conformation and composition of proposed substrate binding loops. Even fewer reports have characterized the function of purified NDM-1, with one publication listing the steady-state kinetic constants for hydrolysis of a set of selected substrates[13] and a second publication reporting IC_{50} values for the thiol-containing inhibitors D- and L-captopril (8 and 200 μM, respectively).[16] This work details the expression and purification of homogeneous monozinc and dizinc metalloforms of NDM-1, the mapping of the N-terminal cleavage site, the determination of metal ion stoichiometry and its influence on catalysis, the characterization of substrate preference, the UV−vis spectra of the dicobalt(II) metalloforms, and molecular modeling of the dinuclear zinc active site. This preparation of homogeneous NDM-1 containing a defined metal content allows a more accurate determination of its function and helps to elucidate the molecular basis for NDM-1-mediated antibiotic resistance.

MATERIALS AND METHODS

Materials. The substrates penicillin G (**1**), ampicillin (**2**), carbenicillin (**3**), cephalexin (**4**), cefaclor (**5**), nitrocefin [**6**, from Beckton Dickinson (Franklin Lakes, NJ)], meropenem (**7**), and imipenem (**8**) and all other chemicals were obtained from Sigma-Aldrich Chemical Co. (St. Louis, MO), unless otherwise noted (Chart 1).

Construction of the Expression Plasmid Encoding a C-Terminal His_6 Affinity Tag. A coding sequence for the NDM-1 produced by strains of *K. pneumoniae* and *E. coli* was synthesized (IDT, San Jose, CA) using codons optimized for expression in *E. coli* (Figure S1 of the Supporting Information). Flanking restriction sites were incorporated using a PCR with the forward primer NDMP1 (5′-tataCATATGgaattgcccaatat-tatgcaccc-3′), which included an *Nde*I restriction site (in capital letters) and the codons for the first six amino acid residues, and the reverse primer NDMP2 (5′-ctgGCTAGCgcgcagcttgtcggc-cat-3′), which included an *Nhe*I restriction site (in capital letters), a stop codon, and codons for the last five amino acid residues of NDM-1. The PCR temperature program was started at 95 °C for 4 min followed by 30 cycles of 30 s at 95 °C, 30 s at 60 °C, and 60 s at 72 °C. The resulting PCR product was purified using a QIAquick kit (Qiagen, Valencia, CA). Both the PCR product and the pET27b(+) expression vector were digested with *Nde*I and *Nhe*I for 2 h at 37 °C, purified using a QIAquick kit, and ligated together to form pET27b-NDM1−6H. A 5 μL aliquot of the ligation mixture was used to transform 50 μL of electrocompetent *E. coli* BL21(DE3) cells, and transformants were selected for growth on solid LB agar plates containing kanamycin (30 μg/mL). Plasmid DNA purified from a single colony was sequenced and confirmed for accuracy of the NDM-1 coding sequence.[2]

Chart 1

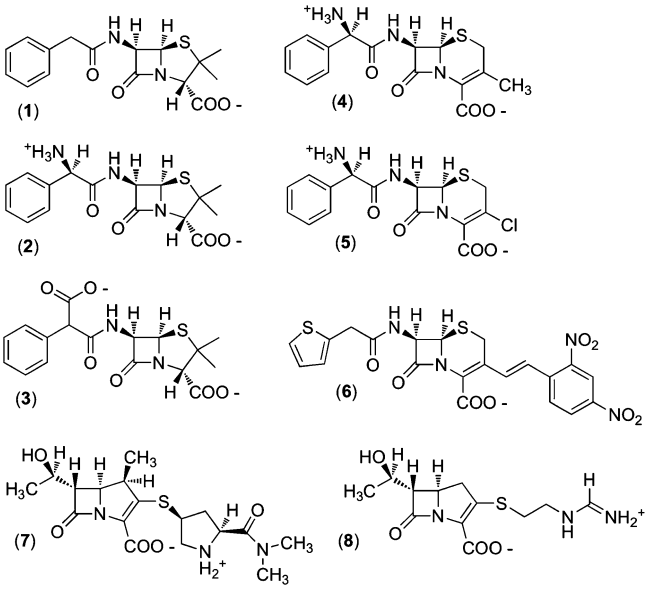

Construction of the Expression Plasmid Encoding an N-Terminal Strep-tag II Affinity Tag. On the basis of analysis of the N-terminal cleavage site found using the native export signal (see below), NDM-1 was recloned to incorporate instead an optimized N-terminal pelB leader sequence [encoded within the pET27b(+) plasmid] to direct export to the periplasm, and an intervening eight-amino acid Strep-tag II affinity tag, followed by a tobacco etch virus (TEV) protease cleavage site, and the NDM-1 coding sequence starting at the sequence encoding residue Gly36. To make this construct, plasmid pET27b-NDM1−6H was used as a template in a PCR along with a forward primer, 5′-tggCCATGG*attggagccacccg-caatttgaaaaggaaaacctgtatttccaa*ggccagcaaatggaaactggc-3′, which contains an *Nco*I cutting site (capital letters) and encodes the Strep-tag II tag and TEV cleavage site sequences (italics) followed by codons for amino acids 36−42 of NDM-1, along with a reverse primer, 5′-ttcGGATCCtcagcgcagcttgtcggccat, which contains a *Bam*HI site (capital letters), codons for the last six amino acid residues of NDM-1, and a stop codon. The PCR program was the same as that described above except that the annealing temperature was 65 °C. The resulting product was digested using *Nco*I and *Bam*HI and subsequently ligated into the corresponding sites of a similarly digested pET27b(+) plasmid. The ligation mixture was then transformed into *E. coli* BL21(DE3) by electroporation and selected for resistant transformants, and the NDM-1 coding sequence was verified as described above for completed expression vector pET27b-Strep-NDM1.

Protein Purification of NDM-1 Using a C-Terminal His_6 Affinity Tag. For protein expression, *E. coli* BL21(DE3) (pET27b-NDM1−6H) cells were cultured by being shaken in 0.5 L of LB medium containing 30 μg/mL kanamycin at 37 °C for approximately 3 h ($Abs_{600} \approx 0.6$) and then cooled to 25 °C before the addition of 0.5 mM IPTG to induce expression. Incubation was continued for 18−20 h at 25 °C, after which cells were pelleted by centrifugation and discarded. NDM-1 bearing a C-terminal His_6 affinity tag (NDM1-His_6) was then purified from the remaining growth medium by using an

immobilized metal affinity chromatography column charged with nickel (HisPur Ni-NTA resin, Thermo Fisher Scientific, Pittsburgh, PA) as follows. The NDM-1-His_6-containing culture medium was filtered through a 0.2 μM membrane, mixed with 10 mL of Ni-NTA resin, gently rocked for 30 min at 4 °C, and then poured into a column. The resulting column was washed with 10 volumes of wash buffer [25 mM KH_2PO_4 (pH 7.6), 300 mM NaCl, and 10 mM imidazole]. The NDM-1-His_6 protein was then eluted using elution buffer (wash buffer with 250 mM imidazole). The eluted protein was dialyzed against 4 L of 25 mM Hepes buffer (pH 7.6) and supplemented with 50 μM $ZnSO_4$ before concentration as described below.

Protein Purification of NDM-1 Using an N-Terminal Strep-tag II Affinity Tag. Using the expression conditions described above, *E. coli* BL21(DE3) (pET27b-Strep-NDM1) was used to produce and secrete soluble affinity-tagged NDM-1 (Strep-NDM-1) into growth medium that had been previously supplemented with 0.05 mM $ZnSO_4$. Purification from LB medium was conducted essentially the same as with M9 minimal medium, which is described below. After expression and removal of cells and cell debris, 1 L of growth medium was transferred into dialysis tubing (molecular weight cutoff of 8000) and overlaid with solid PEG 20000 at 4 °C overnight. As a result, the growth medium is concentrated 3.6-fold. The final solution was diluted with cold deionized water to a total volume of 1.5 L, which decreased the conductivity from 19 to 3.5 mS/cm. The resulting solution was incubated batchwise with 50 mL of DEAE-resin, poured into a column (2.5 cm × 10 cm), subsequently washed with approximately 2.4 column volumes of 25 mM Tris-HCl (pH 7.5) at a rate of 3.0 mL/min, and then eluted using the same buffer with an increasing NaCl concentration (from 0 to 150 mM). The fractions containing lactamase activity (see below for the spectrophotometric kinetic assay) were pooled and loaded onto a GE Healthcare StrepTactin Sepharose affinity column (10 mL), washed with phosphate-buffered saline (PBS), and eluted upon addition of 2.5 mM desthiobiotin. The eluted fractions were pooled and digested with TEV protease, as described previously,[20,21] either in the presence of 1 mM DTT or in the absence of DTT. We note that the inclusion or omission of DTT at this step contributes to the differing metal ion stoichiometry found in the final purified protein (see below). The resulting mixture was loaded onto a Cobalt-NTA (HisPur Cobalt-NTA resin, Thermo Fisher Scientific) column (2.5 cm × 1 cm) equilibrated with 25 mM KH_2PO_4, 0.3 M NaCl, and 10 mM imidazole (pH 7.6) at a rate of 0.5 mL/min to capture the His_6-tagged TEV protease, and to allow the processed, untagged NDM-1 to exit in the flow-through. The column was washed until the Abs_{280} of the flow-through fractions reached a minimum, and these were subsequently pooled and concentrated using an Ultra-10K centrifugal microconcentrating filter (Millipore, Billerica, MA; molecular weight cutoff of 10000) that had been pretreated with *o*-phenanthroline and washed to remove any adventitiously bound metal ions. The same filtration device was used for three buffer exchanges into a final buffer consisting of 50 mM Tris-HCl and 150 mM NaCl (pH 7.5). The final buffer exchange step was completed either using a centrifugal microconcentrator (for monozinc preparations) or by dialysis (for dizinc preparations).

Determining the Metal Ion Content of Purified Enzyme Preparations. Samples (400 pmol) of NDM-1 preparations were analyzed for their metal ion content using inductively coupled plasma mass spectrometry (ICP-MS) (Department of Geological Science, The University of Texas). For each sample, the final flow-through buffer from centrifugal concentration was used as a background control. The numbers of equivalents of bound metal ion were calculated by subtracting the concentration of metal ions found in the control buffer from those found in the protein sample and dividing by the protein concentration.

A second method was also used to determine the zinc ion content for most NDM-1 samples through the use of UV−vis spectrophotometry and a colorimetric chelator, 4-(2-pyridylazo)resorcinol (PAR), in denaturing buffer.[22−24] A standard metal ion solution (50 μL) containing zinc(II) ions (0−60 μM for standard curves) or the protein sample (50 μL) was mixed with 250 μL of PAR and guanidine-HCl to give a final solution of 4.9 M guanidine-HCl, 50 μM PAR, and 0−10 μM metal ion in 61 mM Hepes (pH 7.3). The absorbances of PAR−metal complexes were determined within 5 min using a Cary 50 Bio UV−visible spectrophotometer at 500 nm using quartz cuvettes with a 1.0 cm path length. A standard curve (0−10 μM metal ion) was collected for each series of experimental samples. Protein concentrations were determined using a Bio-Rad Protein Assay kit (Bradford method) and verified by spectrophotometric determination using the molar absorption coefficient (ε_{280}) of NDM-1 at 280 nm in 6 M guanidine-HCl and 75 mM Hepes (pH 7.3). The molar absorption coefficients for Strep-NDM-1 (34850 M^{-1} cm^{-1}, NDM-1 with the N-terminal Strep tag attached) and NDM-1 (27880 M^{-1} cm^{-1}) were calculated using the equation described by Pace et al.[25]

Because PAR is a colorimetric zinc chelator with relatively weak affinity compared to that of EDTA, it was used to treat folded and denatured dizinc NDM-1 to show whether one zinc ion had a weaker affinity for NDM-1 than the other. In a quartz cuvette, 2.5 μL of either a background control buffer [50 mM Tris-HCl and 150 mM NaCl (pH 7.5)] or a dizinc NDM-1 solution (0.5 mM) was mixed with 297.5 μL of a PAR working solution (with or without denaturant) to give a final concentrations of 100 μM PAR and 75 mM Hepes (pH 7.3) with or without guanidinium-HCl (6 M) with or without NDM-1 (4.2 μM). After a 10 min incubation to allow full color development, the UV−vis spectra were recorded.

Spectrophotometric Titration of NDM-1 with Cobalt-(II). A stock solution of dinuclear zinc NDM-1 (6 mg) was diluted to 0.02 mM (15 mL) in 50 mM Hepes (pH 7.0) with addition of EDTA (1 mM) and TCEP (2 mM). After incubation for 30 min on ice and confirmation that NDM-1 was no longer catalytically active, the reaction mixture was concentrated using an Ultra-10K centrifugal microconcentrating filter to approximately 400 μL. Additional buffer and reagents were added to give a solution with a volume of 15 mL containing EDTA (0.5 mM) and TCEP (1 mM). This mixture was again concentrated to give a final solution of apo-NDM-1 (0.38 mM) still with EDTA (0.5 mM) and TCEP (1 mM) present. Aliquots (0.3−1.5 μL each) of a stock solution of $CoCl_2$ (20−200 mM) were added to 360 μL of apo-NDM-1 (0.38 mM), contained in a quartz microcuvette. After the sample had been gently mixed and incubated at 25 °C for 2 min, the absorbance spectrum from 300 to 700 nm was recorded after each addition.

Molecular Modeling. To gain insight into the active site of NDM-1, we have conducted molecular dynamics (MD) calculations using a hybrid quantum mechanical and molecular mechanical (QM/MM) method.[26] The QM/MM approach is essential for zinc enzymes because the force field approach has

so far failed to provide an accurate description of the metal−ligand interactions in zinc enzymes. In this work, the QM region is described by the self-consistent charge density functional tight binding (SCC-DFTB) theory,[27,28] which has been shown to faithfully characterize many MBL active sites.[29−33] The MM region of the enzyme is described by the CHARMM22 all atom force field.[34] The link atom approach was used for the QM−MM interface.[35]

The starting point in our simulations was adapted from the recent X-ray structure of NDM-1 in its dizinc form and complexed with a hydrolyzed ampicillin molecule (PDB entry 3Q6X).[17] We simulated the ligand-free form of the enzyme, which was prepared by removing the hydrolysis product from the enzyme active site. A hydroxide anion is then placed between the two zinc ions, on the basis of previous X-ray structures of dizinc MBLs.[2,3] For comparison, we have also simulated another class B1 MBL, VIM-4, on the basis of a recent X-ray structure of its dizinc form (PDB entry 2WHG).[36] VIM-4 is currently the closest related homologue of NDM-1 for which an X-ray structure has been reported. Because the VIM-4 structure is free of ligand, no modification was performed. The protonation states of all histidine residues were carefully assigned according to the hydrogen bonds with nearby residues. Both models were solvated using a pre-equilibrated TIP3P water[37] sphere with a 25 Å radius centered at a zinc ion (Zn2). This procedure was repeated several times with rotated water spheres to ensure uniform solvation. The solvent was relaxed by 30 ps MD with all protein and substrate atoms fixed. Stochastic boundary conditions[38] were applied to reduce computational costs.

The QM system in these two models consists of the two zinc ions and their protein ligands as well as the bridging hydroxide. Both models were simulated with 1.07 ns MD, with the first 370 ps for heating and equilibration and the rest of the 700 ps trajectories for data analysis. The SHAKE algorithm[39] was employed to maintain covalent bonds involving hydrogen atoms. The integration step for MD simulation is 1 fs.

Determining the Steady-State Rate Constants for Various Substrates. Methods varied slightly depending on the substrate. For nitrocefin, disposable polystyrene cuvettes were used with a final assay volume of 1.5 mL. For all other substrates, quartz microcuvettes were used with a final assay volume of 0.4 mL. Assay buffer contained 50 mM Hepes (pH 7.0) and an optimized $ZnSO_4$ concentration of 10 μM (see below), except where noted. Absorbance changes due to either the disappearance of substrate or the appearance of product were monitored for approximately 0.3 min at 25 °C, adjusting the final concentration of NDM-1 to keep observed rates linear within this time frame. Wavelengths used to monitor turnover of penicillin G, ampicillin, carbenicillin, cephalexin, cafaclor, nitrocefin, meropenem, and imipenem were 235, 235, 235, 265, 265, 485, 300, and 300 nm, respectively. Because the published difference extinction coefficients for some of these substrates were determined using conditions different from those reported here, difference extinction coefficients for each compound were measured using the same buffers used here for kinetic experiments (Table S1 of the Supporting Information). The steady-state K_M and k_{cat} values for each substrate were derived by fitting the concentration dependence of initial rate measurements to the Michaelis−Menten equation using KaleidaGraph (Synergy Software, Reading, PA).

Optimization of Zinc(II) Concentration for Hydrolysis of Various Substrates. Initial rates were determined for hydrolysis of each substrate when stock solutions of the monozinc NDM-1 preparation were added to assay buffer containing variable amounts of $ZnSO_4$, to give a final enzyme concentration between 0.001 and 0.004 μM. When possible, saturating amounts of substrate were used, but lower concentrations were used when the intrinsic absorbance of the substrate was too high, resulting in a range of substrate concentrations (in parentheses) from 2- to 23-fold greater than each respective substrate's K_M value: penicillin G (1 mM), ampicillin (1 mM), carbenicillin (800 μM), cephalexin (20 μM), cefaclor (20 μM), nitrocefin (30 μM), imipenem (150 μM), and meropenem (150 μM).

RESULTS

Protein Purification of NDM-1 Expressed with Its Native Leader Sequence. The native NDM-1 sequence includes an export leader sequence, although the exact cleavage site(s) is not clear. Therefore, to experimentally map sites of posttranslational cleavage after export, we initially expressed NDM-1 containing its native leader sequence. Using our overexpression system, protein solubility appeared to be temperature-dependent. Induction of protein expression at 37 °C for 2 h resulted in accumulation of an insoluble cytoplasmic protein that matched the expected size of NDM-1, as measured by sodium dodecyl sulfate−polyacrylamide gel electrophoresis (SDS−PAGE). In contrast, after induction at 25 °C for 18 h, soluble NDM-1 was apparent in both the cytoplasmic fractions and the growth medium. Using these conditions, 4 mg of purified NDM-1-His_6 could be isolated from 0.5 L of growth medium using a single-step Ni-NTA affinity column.

Mapping the N-Terminal Processing Site. Purified NDM-1-His_6 appeared to be homogeneous by Coomasssie-stained SDS−PAGE and migrated with an apparent molecular mass of approximately 28 kDa. Analysis of the purified protein by ESI-MS (Analytical Core Facility, College of Pharmacy, The University of Texas) revealed four major peaks with the approximate relative abundance of each peak listed here in parentheses, assuming similar ionization efficiencies for each species: 29171 Da (21%), 28927 Da (30%), 28896 Da (23%), and 27204 Da (26%). These values are consistent with cleavage of the protein's prosequence after residues 15, 17, 18, and 35, respectively. Cleavage after residue 35 produces the shortest protein and is most consistent with the length of structured regions observed by X-ray crystallography of similar MBLs. The heterogeneity of multiple cleavage sites and the use of a His_6 affinity tag for purification were potential interfering factors when obtaining a homogeneous metalloenzyme. Therefore, an expression construct containing a deletion of the first 35 residues and incorporation of an alternative affinity tag was used for the remaining experiments.

Protein Purification of NDM-1 Using an N-Terminal Strep-tag II Affinity Tag. The alternatively tagged version of NDM-1 is initially expressed with an N-terminal pelB leader sequence (derived from the expression plasmid) that is subsequently used and cleaved during culturing to release Strep-NDM-1 into the growth medium. The resulting protein contains a short (eight-amino acid) N-terminal Strep II affinity tag followed by a TEV protease digestion site, and then residue Gly36 (and the following residues) of the NDM-1 enzyme. Initial expression trials conducted using 0.5 L of LB medium showed that approximately 80% of the protein found in the medium had a molecular mass that was the same as that expected for Strep-NDM-1. Addition of 50 μM $ZnSO_4$ to the

growth medium increased the level of expression approximately 2-fold and disproportionally also increased total activity by approximately 17-fold. Further optimization of growth conditions to best balance yield and protein homogeneity resulted in the use of M9 minimal medium supplemented with 50 μM $ZnSO_4$ for the remaining studies (unless specified). Using these culturing conditions, more than 50% of all protein found in the growth medium was Strep-NDM-1 (Figure 1).

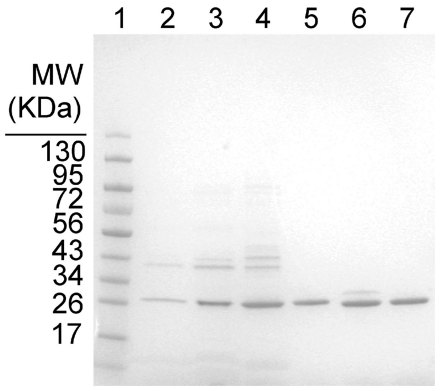

Figure 1. NDM-1 purification. Gradient SDS–PAGE (4 to 20%) gels, Coomassie-stained, show protein bands at various stages of the purification: lane 1, molecular mass standards; lane 2, growth medium after expression; lane 3, concentrated growth medium; lane 4, after DEAE chromatography; lane 5, after StrepTactin affinity chromatography; lane 6, after digestion with TEV protease (upper band); lane 7, flow-through from the Cobalt-NTA column.

Concentration of the cell-free culture medium followed by two column chromatography steps, TEV protease cleavage of the affinity tag [completed in the presence or absence of DTT (see below)] and affinity chromatography to capture TEV protease, and subsequent concentration of the final protein yielded approximately 10 mg of untagged NDM-1 from 1 L of initial culture. Gel filtration of purified NDM-1 shows an elution time consistent with a monomeric protein (Figure S2 of the Supporting Information). We note that, using similar procedures, NDM-1 can also be purified directly from whole cells in even greater yields (Figure S3 of the Supporting Information).

Identity and Stoichiometry of Bound Metal Ions in NDM-1 Preparations. After purification from the medium of cultures grown in LB medium, using the standard procedures described above that include DTT in the affinity tag cleavage step, NDM-1 is purified to near homogeneity and is found to contain 1 equiv of zinc ion (Table 1). Expression cultures grown in M9 minimal medium produced a lower protein yield, but the resulting protein also contained a slightly lower abundance of contaminating iron and nickel ions. Therefore, $ZnSO_4$-supplemented M9 medium was chosen for optimal expression and purification. As in other reports,[16] we found that addition of EDTA rapidly results in a total loss of activity and can be used to prepare the apoenzyme. No NDM-1 activity is detected in EDTA-treated samples, but minor amounts of activity and 0.2 equiv of zinc ion are inadvertently recovered in the following purification steps that remove excess metal ion chelator (Table 1).

Although examples of both mononuclear and dinuclear zinc MBLs are known, we investigated whether this monozinc NDM-1 metalloform was likely the native form of the enzyme or was formed, at least in part, because of our particular purification procedure. Toward this end, Strep-NDM-1, a form of NDM-1 that still contains the N-terminal affinity tag, was examined for metal ion content and was found instead to contain 1.8 equiv of zinc ion (Table 1). Therefore, several experimental steps following this stage of purification were modified to determine if they impacted the metal ion content in the final purified protein. Through this process, it was discovered that if DTT is omitted from the purification step in which TEV protease cleaves the N-terminal affinity tag, and if the final buffer exchange step is completed by dialysis instead of by a centrifugal microconcentrator, then the final purified untagged NDM-1 protein instead contains 1.8 equiv of zinc ion.

Initial tests of enzyme activity with ampicillin, nitrocefin, and meropenem substrates showed similar behaviors of monozinc and dizinc NDM-1 stock solutions once they were diluted for kinetic assays (not shown). A possible explanation for this behavior is that one of the zinc ions is bound more loosely than the other and dissociates upon dilution. Therefore, we investigated whether PAR, a colorimetric zinc chelator with a relatively weak affinity for zinc, could remove zero, one, or two metal ions from the dizinc NDM-1 preparation (Figure 2). Upon incubation of PAR (100 μM) with natively folded, dizinc NDM-1, an increase in absorbance at 500 nm is observed, which is indicative of PAR chelating zinc ions. The magnitude of the absorbance change is converted to equivalents of chelated zinc using a standard curve and the protein concentration of NDM-1 and reveals that PAR chelates 1.0 equiv of zinc ion that was taken from the dizinc NDM-1 stock under these conditions. The same experiment was then repeated in the presence of denaturant to unfold dizinc NDM-1, and the resulting increase in absorbance at 500 nm indicates that PAR chelates 1.9 equiv of zinc ion that was released from unfolded NDM-1.

UV–Vis Spectroscopy of Reconstitution of NDM-1 with Cobalt(II). To obtain solution-phase information about

Table 1. Metal Ion Content of Various NDM-1 Preparations

protein	preparation	zinc	cobalt[f]	iron[f]	nickel[f]
NDM-1	LB and zinc[a]	1.0[f,g]	<0.1	0.1	0.1
NDM-1	M9 and zinc[b]	1.0[f,g]	<0.1	<0.1	<0.1
NDM-1	apo[c]	0.2[f]	<0.1	<0.1	<0.1
Strep-NDM-1[d]	M9 and zinc	1.8[f,g]	<0.1	<0.1	<0.1
NDM-1	M9 and zinc (without DTT)[e]	1.8[g]	ND[h]	ND[h]	ND[h]

[a]From expression cultures using LB medium supplemented with $ZnSO_4$. [b]From expression cultures using M9 minimal medium supplemented with $ZnSO_4$. [c]Apoprotein resulting from treatment with a metal chelator and subsequent dialysis. [d]Uncleaved fusion protein Strep-NDM-1 after purification by StrepTactin affinity chromatography. [e]DTT was omitted during the TEV protease digestion step. [f]Metal ion content determined by ICP-MS. [g]Zinc ion content determined using PAR. [h]Not determined.

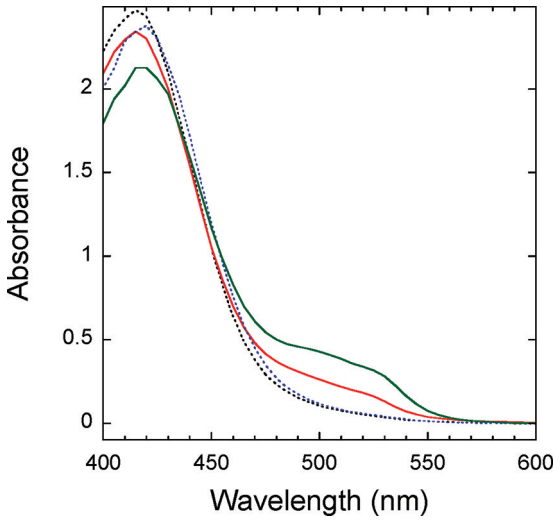

Figure 2. Probing zinc stoichiometry using PAR. For control samples, spectra are shown for the colorimetric zinc chelator PAR in background buffer in the absence (black dashed line) and presence of guanidinium-HCl denaturant (blue dashed line). For the experimental samples, spectra are shown upon addition and incubation (10 min) of a dizinc NDM-1 stock solution (4.2 μM) with background buffer in the absence (solid red line) or presence (solid green line) of denaturant. The extent to which an increase in absorbance at 500 nm is observed reflects PAR chelation of 1.0 equiv of zinc from folded NDM-1 and 1.9 equiv of zinc from denatured NDM-1.

the active site metal ion cluster of NDM-1 for comparison with released X-ray crystal structure coordinates, spectra of a cobalt(II) titration of apo NDM-1 were recorded. However, initial studies indicated that apo NDM-1 is susceptible to oxidation; ESI-MS of monozinc NDM-1 showed the expected mass for the unmodified enzyme, but apo NDM-1 showed masses consistent with multiple oxidation events (data not shown) and was found to be unsuitable for metal reincorporation experiments. Therefore, to minimize experimental handling of the apoprotein, the cobalt(II) titration was performed by using dizinc NDM-1 that was treated with EDTA and then, directly in the same solution, treated with increasing additions of a cobalt(II) salt. Briefly, an EDTA-treated, zinc-depleted NDM-1 (0.38 mM) solution that still contains supplemental TCEP (1 mM) and EDTA (0.5 mM) was treated with aliquots of $CoCl_2$. As expected, addition of cobalt(II) did not result in any obvious changes to the difference spectrum until the concentrations were >0.5 mM (Figure 3). Then, increasing $CoCl_2$ concentrations led to formation of four obvious peaks that occur at 330, 510, 549, 615, and 640 nm. The heights of these peaks appear to increase at similar cobalt(II) concentrations, reaching their maxima at approximately 1.6 mM $CoCl_2$. The molar extinction coefficient for the 330 nm band was measured to be 930 M^{-1} cm^{-1}. The four remaining peaks are not as well resolved, with the highest peak at 549 nm showing a molar extinction coefficient of 400 M^{-1} cm^{-1}.

Molecular Modeling. To improve our understanding of the active site structure and dynamics of NDM-1, we have conducted QM/MM MD simulations of NDM-1 in its dizinc form without an active site ligand. For comparison, we have also simulated VIM-4, the sequence of which is approximately 35% identical with that of NDM-1. As shown in Figure 4, both structures are quite stable, as evidenced by the rmsd (root-

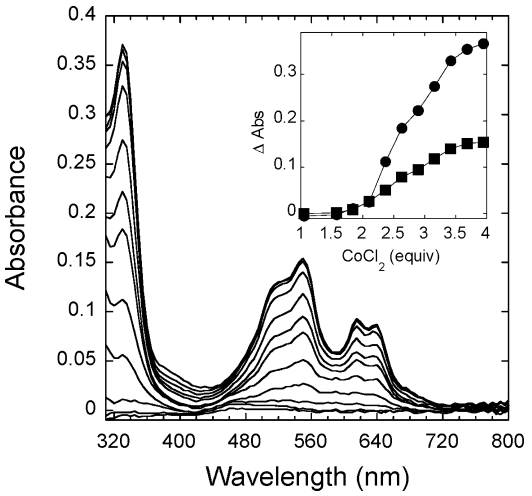

Figure 3. Difference UV−vis spectra of apo NDM-1 titrated with $CoCl_2$. NDM-1, depleted of metal ions by EDTA (0.5 mM) treatment, is titrated with $CoCl_2$ (0.4, 0.6, 0.7, 0.8, 0.9, 1.0, 1.1, 1.2, 1.3, 1.4, 1.5, and 1.6 mM), and the difference spectra are shown for each, resulting in increases in absorbance at 330, 510, 549, 615, and 635 nm. The inset shows the changes in absorbance at 330 (●) and 550 nm (■) upon titration of $CoCl_2$. These experiments were completed in the presence of 1.3 equiv (0.5 mM) of EDTA.

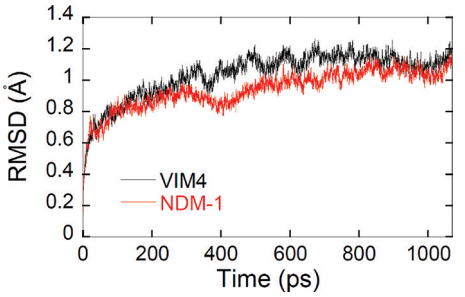

Figure 4. Root-mean-square deviations (RMSD) for NDM-1 (1.00 ± 0.07 Å) and VIM-4 (1.12 ± 0.05 Å).

mean-square deviation). The two zinc ions are well-ligated by protein residues (Figure 5). Specifically, one zinc ion is ligated

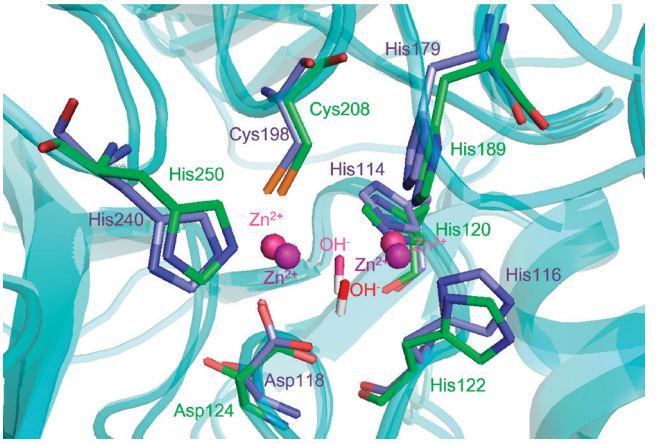

Figure 5. Overlay of NDM-1 (green carbon atoms, purple zinc ions, and red hydroxide ion) and VIM-4 (light blue carbon atoms, pink zinc ions, and pink hydroxide ion). Both structures were randomly selected from MD simulations of the respective proteins.

dx.doi.org/10.1021/bi201449r | *Biochemistry* 2011, 50, 10102–10113

Table 2. Selected Geometries of NDM-1 and VIM-4 Obtained from QM/MM MD Simulations[a]

NDM-1			VIM-4		
distance (Å)	MD[b]	EXP[c] (ref 17)	distance (Å)	MD[b]	EXP[c] (ref 36)
Zn1···Nε2(His189)	2.00 ± 0.05	2.04	Zn1···Nε2(His114)	2.03 ± 0.06	2.10
Zn1···Nδ1(His122)	2.01 ± 0.05	1.99	Zn1···Nδ1(His116)	2.00 ± 0.06	2.05
Zn1···Nε2(His120)	2.03 ± 0.06	2.11	Zn1···Nε2(His179)	1.98 ± 0.05	2.05
Zn1···Ow	2.01 ± 0.06	2.02	Zn1···Ow	2.00 ± 0.06	1.88
Zn1···Zn2	3.58 ± 0.11	4.59	Zn1···Zn2	3.57 ± 0.11	3.85
Zn2··· Ow	2.02 ± 0.06	2.99	Zn2···Ow	2.02 ± 0.06	2.40
Zn2···Nε2(His250)	2.01 ± 0.06	2.02	Zn2···Nε2(His240)	2.01 ± 0.06	2.14
Zn2···Oδ1(Asp124)	2.14 ± 0.07	2.15	Zn2···Oδ1(Asp118)	2.18 ± 0.08	2.07
Zn2···Sγ(Cys208)	2.34 ± 0.07	2.35	Zn2···Sγ(Cys198)	2.32 ± 0.06	2.41
H1···Oδ2(Asp124)	2.13 ± 0.40	–	H1···Oδ2(Asp118)	1.97 ± 0.30	–
Ow···Oδ2(Asp124)	2.87 ± 0.18	2.48	Ow···Oδ2(Asp118)	2.79 ± 0.13	3.52
Zn2···Nζ(Lys125)	5.45 ± 0.27	5.93	Zn2···Cζ(Arg119)	4.31 ± 0.21	4.67

[a]Distances determined from crystallographic structures are included for comparison. [b]Distances determined by molecular dynamics simulations. The distances given are the averages and standard deviations for each measurement over the entire time trajectory. [c]Distances determined by experimental measurements, as referenced.

by three His residues in the so-called metal 1 site (M1), while the second zinc ion is bound by a His, a Cys, and an Asp at the so-called metal 2 site (M2), thereby forming a dinuclear zinc ion cluster at the active site. The metal–ligand distances are quite close to their experimental counterparts, as shown in Table 2. The bridging hydroxide ion is roughly equidistant to both zinc ions, and hydrogen bonded to the zinc-binding Asp residue (Asp124 in NDM-1 and Asp118 in VIM-4). Interestingly, the Zn1–Zn2 distance in our ligand-free NDM-1 model is significantly shorter than in the X-ray structure, which has hydrolyzed ampicillin at the active site.[17] The ligand-free model of NDM-1 has a Zn1–Zn2 distance (3.58 ± 0.11 Å) that is very similar to that in VIM-4 (3.57 ± 0.11 Å), which is in reasonably good agreement with experimental values for that enzyme (3.85 Å).[36] Finally, Lys125 is close to Zn2 in NDM-1, with an average Nε–Zn2 distance of 5.87 ± 0.20 Å. Cationic residues at this position have been proposed to be (at least partially) responsible for the lower affinity of metal ions in the M2 site (see below). In VIM-4, an Arg residue (Arg119) is in the same structural position, and its distance to Zn2 is even shorter (4.31 ± 0.21 Å). Snapshots of the active site models of the two enzymes are displayed in Figure 5. The active site models emerging from these simulations are consistent with our earlier work on homologous dizinc enzymes.[30−32]

Optimization of the Zinc(II) Concentration for Hydrolysis of Various Substrates. To improve our understanding of how zinc ion stoichiometry impacts function, we investigated the ability of increasing $ZnSO_4$ concentrations in assay buffer to complement the activity of monozinc NDM-1 stock solutions when used to hydrolyze three different classes of substrates (Figure 6). Penams (**1**–**3**) were hydrolyzed at only 30–50% of their maximal hydrolysis rates when no additional $ZnSO_4$ was added, and the rates were maximal near 10 μM $ZnSO_4$; a subset of these substrates showed decreased hydrolysis rates at increased $ZnSO_4$ concentrations. Cephem (**4**–**6**) hydrolysis rates were found to be less sensitive to $ZnSO_4$ concentrations in assay buffer, with values only ranging between 80 and 100% of maximal activity. Finally, the two carbapenems (**7** and **8**) tested showed differing results, with imipenem showing little sensitivity to $ZnSO_4$ concentrations but meropenem showing significantly decreased activity at higher $ZnSO_4$ concentrations. Of all of the substrates tested, a $ZnSO_4$ concentration of approximately 10 μM in assay buffer resulted in maximal observed rates and so was used to compare substrate preferences. Experiments starting instead with a dizinc NDM-1 stock solution showed similar results, although the zinc concentrations required for the maximal rates were slightly shifted, possibly because of differing starting zinc concentrations carried over from the initial enzyme stock solution (data not shown).

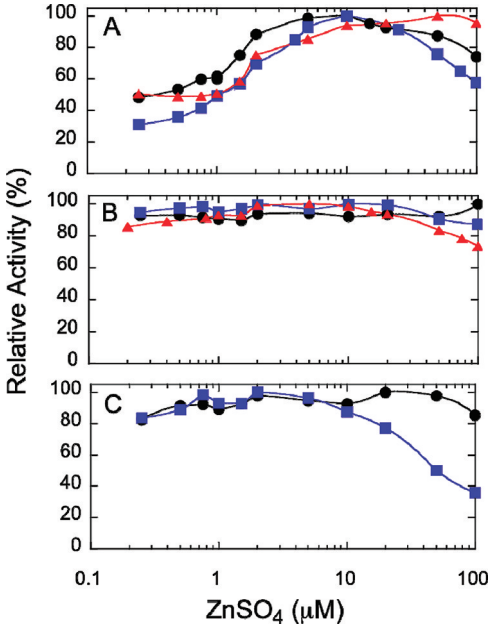

Figure 6. Zinc dependence of NDM-1-catalyzed hydrolysis of various substrates. Measurements were taken at substrate concentrations that were greater than the K_M using an NDM-1 stock bound to 1 equiv of zinc, with increasing $ZnSO_4$ concentrations in the assay solution. See Materials and Methods for full details. (A) Penems: penicillin G (black circles), ampicillin (blue squares), and carbenicillin (red triangles). (B) Cephems: cephalexin (black circles), cefaclor (blue squares), and nitrocefin (red triangles). (C) Carbapenems: imipenem (black circles) and meropenem (blue squares). Approximately 10 μM $ZnSO_4$ added to assay buffer results in near-maximal activity for all substrates tested.

Steady-State Rate Constants for Various Substrates. The k_{cat} and K_M values for eight substrates were determined (Table 3) starting with those of a monozinc NDM-1 stock solution that was supplemented with $ZnSO_4$ (10 μM) in assay

Table 3. Steady-State Rate Constants for NDM-1 and Various Substrates, Assayed in 10 μM $ZnCl_2$

substrate class	substrate	K_M (μM)	k_{cat} (s^{-1})	k_{cat}/K_M (M^{-1} s^{-1})
penem	penicillin G (**1**)	240 ± 50	720 ± 50	3.0×10^6
penem	ampicillin (**2**)	310 ± 30	690 ± 30	2.2×10^6
penem	carbenicillin (**3**)	410 ± 40	570 ± 20	1.4×10^6
cephem	cephalexin (**4**)	5.6 ± 0.4	47 ± 1	8.4×10^6
cephem	cefaclor (**5**)	1.8 ± 0.2	36 ± 1	2.0×10^7
cephem	nitrocefin (**6**)	1.3 ± 0.2	15.4 ± 0.4	1.2×10^7
carbapenem	meropenem (**7**)	54 ± 3	138 ± 3	2.6×10^6
carbapenem	imipenem (**8**)	45 ± 2	195 ± 3	4.3×10^6

buffer to reflect optimal activity levels. All three classes of β-lactams tested, penems, cephems, and carbapenems, were excellent substrates for NDM-1, with k_{cat}/K_M values ranging from 1.4×10^6 to 2.0×10^7 M^{-1} s^{-1}. Cephems have the lowest K_M values. Carbapenems have K_M values that are 1 order of magnitude higher, and penems have values that are yet an additional 1 order of magnitude higher. The trend of k_{cat} values somewhat offsets these differences (penems > carbapenems > cephems). Therefore, taken together, the substrate preference of NDM-1 determined with optimal zinc content can be reflected in the order of the k_{cat}/K_M values: cephems (10^7 M^{-1} s^{-1}) > carbapenems (10^6 M^{-1} s^{-1}) ≥ penems (10^6 M^{-1} s^{-1}).

To determine if zinc supplementation of assay buffer has the same effect on NDM-1 that was purified as the dizinc form as it did on the monozinc form, stock solutions of both monozinc and dizinc metalloforms were used to measure k_{cat} and K_M values for three representative substrates, nitrocefin, ampicillin, and meropenem, in the presence of supplemental $ZnSO_4$ (10 μM) in assay buffer. In every case, the k_{cat}/K_M values determined from zinc-supplemented reaction mixtures starting with either the monozinc or the dizinc NDM-1 stock solutions were the same, within error (Table S2 of the Supporting Information).

DISCUSSION

To biochemically characterize the antibiotic resistance determinant NDM-1, we first sought to purify a homogeneous preparation. Native NDM-1 is expressed with an N-terminal signal peptide[13] that allows shuttling of the enzyme into the periplasmic space where it can effectively deactivate β-lactam antibiotics. Different algorithms have predicted cleavage of this signal sequence prior to different residue positions: Ala19,[13] Gly29,[17] or a Cys26 that is also predicted to be lipid-modified.[18] NDM-1 has also been intentionally cloned to encode deletions of the N-terminus prior to residue Met27 or Gly47 to improve crystallization.[16,18] Because NDM-1 has been found in clinically isolated *E. coli* strains, we sought to experimentally map the major processed form of recombinant NDM-1 that is expressed with its native leader sequence in a laboratory strain of *E. coli*, BL21(DE3) (pET27b-NDM1−6H). Mass spectrometry of active NDM-1 purified directly from the culture medium revealed several different masses, consistent with NDM-1 having a ragged N-terminus with cleavage sites prior to residues Ala16, Ala18, Ala19, and Gly36, which could result from initial cleavage by a signal peptidase and possibly other processing. Because NDM-1 is produced naturally in Enterobacteriacea, it is possible that heterogeneous processing may be a feature also found in resistant isolates, although assessment of any functional impact will require further study. A lipid-modified form of NDM-1[18] was not identified, but this result is not unexpected because any lipidated forms are not expected to be released into the surrounding culture medium. Because cleavage prior to Gly36 produces the smallest protein that is closest in size to the structured regions observed for NDM-1 and other group B1 MBLs by X-ray crystallography, this truncation was selected for further study. Accordingly, the 35-residue N-terminal deletion from NDM-1 was recloned to instead incorporate a vector-derived pelB leader sequence that is optimized for export and subsequent cleavage of periplasmic proteins in *E. coli*, and this construct was used for all further experiments (Figure 1).

The oligomeric state of NDM-1 is reported to be either monomeric[13,16] or (partially) dimeric.[18] Dimerization of NDM-1 is proposed to occur, in part, through a loop insert (Thr162−Gly167)[18] unique to NDM-1,[13] which contributes to the proposed dimerzation interface as visualized in two separate crystal structures.[17,18] In contrast, the purification method described herein produces NDM-1 that elutes from a gel filtration column with an apparent molecular mass near 24 kDa, which is most consistent with classifying NDM-1 as monomeric and is also consistent with other reports of NDM-1's monomeric state (Figure S2 of the Supporting Information).[13,16,19] The only apparent difference between the protein studied here and that of dimeric NDM-1 is the length of the N-terminus and its possible lipidation. The protein studied here has a 35-residue deletion, but the form used in the dimerization studies was full-length and contained a proposed lipidation modification.[18] Therefore, we can conclude that although the unique NDM-1 loop insert found between residues Thr162 and Glu167 may contribute to dimerization, it is not sufficient by itself to enforce dimerization without additional interactions mediated either by the N-terminal extension or by membrane anchoring through lipidation. Future studies will address any effect the possible lipidation and dimerization may have on the activity of NDM-1 and its ability to confer antibiotic resistance.

The MBL superfamily of proteins is quite diverse in the identity and stoichiometry of its bound metal ions. The best-studied examples have two zinc ions bound in a dinuclear active site cluster; however, more exotic examples can include iron or manganese ions, and the number of bound metal ions can range between zero and three, although these are not always bound at the active site.[40−46] On the basis of its primary sequence, NDM-1 is classified as a group B1 MBL,[13] a group that generally contains a dinuclear zinc cluster at the active site but also contains examples for which the affinities of the two zinc ions differ sufficiently to favor the monozinc form.[5,41,47,48] To date, most reported structures of NDM-1 contain a dinuclear metal ion cluster at the active site,[16−18] with one exception. One report shows a monozinc NDM-1 in which the M1 site (containing ligands His120, His122, and His189) is occupied by a zinc(II) ion but the M2 site (containing ligands Asp124, Cys208, and His250) is not occupied by a metal ion.[19] Also, a

diffierent structure of NDM-1 shows a dizinc ion cluster with a higher *B* factor for the M2 site than the M1 site along with a total zinc content of 1.5 equiv.[18] The method reported herein results in purification of NDM-1 containing 1.8 equiv of zinc ion, which is most consistent with the reported dizinc structures (Table 1). However, we also serendipitously found that minor alterations of the purification procedure result in purification of NDM-1 that contains only 1.0 equiv of zinc ion, indicating that monozinc NDM-1 can also be prepared (Table 1).

We then tested the hypothesis that dizinc NDM-1 contains one zinc binding site that has less affinity than the second zinc binding site, by using the zinc chelator PAR, which can colorimetrically quantify the concentration of chelated zinc ions. When natively folded dizinc NDM-1 is mixed with PAR, only 1 equiv of zinc ion is bound by PAR (Figure 2). However, when unfolded dizinc NDM-1 is treated, 2 equiv of zinc ion are bound by PAR. Treatment with EDTA results in complete removal of both zinc ions from dizinc NDM-1, but the relatively weaker chelator PAR is only apparently able to pull out 1 equiv of zinc, leaving behind a second more tightly bound zinc ion that is only released upon protein denaturation. Therefore, these results are consistent with the proposal that NDM-1 has two zinc binding sites that have different affinities. Comparison of the NDM-1 structure with other group B1 MBLs suggests one possible reason for the differing affinities. In the case of *B. cereus* MBL, which has one tight binding (M1 site) and one loose binding (M2 site) zinc site, Arg121 (*B. cereus* numbering) is placed adjacent to the M2 site. The presence of a positively charged residue at this structural position has been proposed to contribute, at least partially, to the weaker affinity of the M2 site.[41] Although selected mutations at this residue in the *B. cereus* MBL did not result in an increase in metal ion affinity at the M2 site,[49] the converse was shown in a homologue. Mutation of *Bacteroides fragilis* MBL to introduce a positively charged residue into the same structural position converts this normally dizinc enzyme into a variant with a lower-affinity M2 site.[22] Notably, VIM-4, which shows a higher level of overall sequence identity to NDM-1, also has an Arg residue at the same structural position and shows a concentration-dependent relationship between exogenous zinc ions and enzyme activity that is quite similar to that of NDM-1 (see below).[36] In agreement with these correlations, NDM-1 has a positively charged residue, Lys125 (NDM-1 numbering), at the same structural position as MBLs that have a lower-affinity M2 site. Therefore, these correlations suggest that the M2 site of NDM-1 is the site with weaker zinc ion affinity and are consistent with the published monozinc (M1 site) NDM-1 structure.[19]

In an effort to gain more information about the metal ion binding sites from solution-phase experiments, we titrated metal-depleted NDM-1 with cobalt(II) ions (Figure 3). Two notable features were observable in the difference spectra. The first is the formation of a series of four absorbance peaks found between the wavelengths of 448 and 680 nm, which are characteristic of cobalt(II) d−d transitions. Typically, the magnitude of these extinction coefficients is >300 M^{-1} cm^{-1} for four-coordinate cobalt(II), approximately 100−150 M^{-1} cm^{-1} for five-coordinate cobalt(II), and even less (<30 M^{-1} cm^{-1}) for six-coordinate cobalt(II).[50−53] For NDM-1, the measured extinction coefficient for the highest peak at 549 nm is 400 M^{-1} cm^{-1}. Therefore, in this regard, the spectra of cobalt-substituted NDM-1 can be interpreted as being consistent with the published X-ray structures of dizinc NDM-1 that shows a four-coordinate M1 site and a five-coordinate M2 site. The second obvious feature in the cobalt(II) difference spectra is appearance of a peak at 330 nm with an extinction coefficient of 950 M^{-1} cm^{-1}. This band is indicative of a ligand-to-metal charge transfer (LMCT) band, which is typically observed for cobalt(II)−thiolate interactions and is quite similar to that reported for the homologous enzyme IMP-1 (ε_{350} = 1200 M^{-1} cm^{-1}).[54] This observation is consistent with X-ray crystal structures of NDM-1 that show Cys208, the only remaining Cys residue in processed NDM-1, is a M2 site ligand. However, both d−d transition bands, which are dominated by a four-coordinate interaction, and the LMCT band, which is due to interaction with Cys208, appear and are saturated at similar concentrations of added cobalt(II) (Figure 3, inset). This is an unexpected result if the four-coordinate M1 site has a significantly higher metal ion affinity than the five-coordinate Cys-containing M2 site, as proposed above. This result suggests that NDM-1 has different relative affinities for cobalt(II) and zinc(II) ions, that cobalt ions, unlike zinc, bind cooperatively, or that cobalt (II) ions express a ligand preference different from that of zinc. Consistent with this last idea is a set of released coordinates for an NDM-1 that is substituted with the more thiophilic metal ion, cadmium(II), in which one crystallographic monomer shows the Cys208 residue placed equidistant from each of the two active site cadmium ions, demonstrating that a difference in the primary coordination shell can be achieved upon alternative metal ion substitution (PDB entry 3SRX, chain B).

The primary coordination sphere of the active site dinuclear zinc cluster even shows some variations between X-ray crystal structures determined by separate laboratories. For example, the 2.1 Å resolution structure of uncomplexed dizinc NDM-1 reported by King and Strynadka shows a primary coordination sphere around each metal ion site that is typical for class B1 MBLs.[18] However, the 2.5 Å resolution structure of uncomplexed dizinc NDM-1 reported by Guo et al. has a primary coordination shell around each metal ion that significantly deviates from typical M1 and M2 sites in terms of the distance and conformation of the coordinating ligands.[16] Therefore, to improve our understanding of the binding and dynamics of the biologically relevant dizinc ion cluster found at the active site of NDM-1, we used a molecular modeling approach.

As a starting point for molecular modeling, the 1.3 Å resolution structure of NDM-1 in complex with a reaction product was selected.[17] Although our simulations were ultimately conducted in the absence of a docked substrate or product, this starting point was selected because of its improved resolution and to ensure that the crystallized protein represents a form of the active protein (as reflected by conversion of substrate to the observed product during cocrystallization). QM/MM MD studies were able to simulate a stable uncomplexed dizinc NDM-1, and parallel studies with models of VIM-4 gave similar results (Figures 4 and 5). Notably, the zinc primary coordination shells in modeled NDM-1 were consistent with those observed experimentally with most class B1 MBL crystal structures and are more consistent with the uncomplexed structure reported by King and Strynadka rather than that of Guo et al.,[16,18] as reflected in the placement of the primary coordinating residues and the bridging hydroxide. Specifically, the Zn1−Zn2 distance in simulated NDM-1 (3.6 Å) is considerably shorter than that of the product-bound

structure (4.6 Å). However, the model's difference matches quite closely that observed in uncomplexed dizinc NDM-1 by King and Strynadka (3.6 Å). This increase in distance upon product binding is consistent with the observed loss of the hydroxide ion "bridge" and is likely an indication that a "breathing" motion occurs between the two zinc ions during turnover, rather than just a crystallization artifact. Indeed, the Zn1−Zn2 distance has been shown to vary between 3.42 and 3.62 Å throughout the normal catalytic mechanism in a related class B3 MBL.[55] Because of the structural similarities between our models and those of other class B1 MBLs (Table 2 and Figure 5), it is reasonable to propose that the dizinc form of NDM-1 uses a catalytic mechanism similar to that proposed for other class B1 MBLs.[3]

Because monozinc and dizinc metalloforms of NDM-1 can be prepared, we characterized the effect of zinc content on NDM-1 function. Monozinc NDM-1 was supplemented with varying concentrations of zinc to monitor any resulting differences in activity. Specifically, the effect of zinc concentration on hydrolysis rates of saturating (or near-saturating) concentrations of various substrates was found to be highly dependent on the substrate structure (Figure 6). Hydrolysis rates for penem substrates, such as penicillin G, ampicillin, and carbenicillin, showed the greatest increases upon zinc supplementation, displaying an improvement of as much as 320%. Zinc supplementation had a much weaker effect on the hydrolysis rates for cephem substrates, with only modest increases observed for cephalexin, cefaclor, and nitrocefin. The carbapenems imipenem and meropenem also showed only modest increases in hydrolysis rates upon zinc supplementation. Notably, certain substrates in each class also show a decrease in observed rates as zinc concentrations increased to 100 μM, with the most drastic loss in activity being that observed for meropenem. Similar zinc-dependent activity behavior has been recently reported for VIM-4.[36] Because the experiments with NDM-1 were completed here using saturating substrate conditions, the differential effects of zinc supplementation with respect to the three classes of β-lactams used likely reflect dissimilar contributions of the second metal ion toward catalysis of the hydrolysis of these substrates. However, caution should be used when assigning these contributions to a zinc ion bound at a particular metal ion site (e.g., the M1 or M2 site). Vila and co-workers have elegantly demonstrated that, in at least one monometal MBL, the single metal ion exists in equilibrium between the M1 and M2 sites in the resting enzyme but can favor binding at the M2 site during substrate turnover.[56] Therefore, the specific role of each metal ion site in monozinc NDM-1 catalyzed hydrolysis is difficult to predict without more detailed studies.

Regardless of the exact catalytic mechanism, fitting the zinc concentration dependence of penem hydrolysis rates allows the approximation of 2 μM for the K_d value for the more weakly bound zinc ion (Figure S4 of the Supporting Information). This value is consistent with the ability of PAR to sequester this more weakly bound zinc, and with the binding constants reported for homologous class B1 MBLs.[54] This weaker binding site can be readily supplemented with exogenous zinc. NDM-1 catalyzed hydrolysis of all the substrates tested and displayed maximum rates with supplemental ~10 μM zinc, so these conditions are used to determine the steady-state rate constants for eight representative substrates to allow a rank order comparison of substrate preference based on k_{cat}/K_M values (Table 3). These values, whether they were obtained by starting with a monozinc or dizinc NDM-1 stock solution (Table S2 of the Supporting Information), are within error of each other for each substrate, likely reflecting the ability of monozinc NDM-1 to rapidly reincorporate a second zinc ion from solution. β-Lactams from each structural class tested, including penems, cephems, and carbapenems, were all excellent substrates with high catalytic efficiency, displaying k_{cat}/K_M values ranging from 1.4×10^6 to 2.0×10^7 M^{-1} s^{-1}, with a slight preference shown for cephem substrates. Although NDM-1 displays a balanced selectivity between these classes of substrates, the similar k_{cat}/K_M values are achieved through different means. In general, the K_M values for cephems are 17-fold lower than those of carbapenems and 110-fold lower than those of penems, but each class has offsetting k_{cat} values, resulting in their similar specificity constants. These results differ somewhat from the smaller k_{cat}/K_M values (ranging from 2×10^4 to 1×10^6 M^{-1} s^{-1}) and different ranking of substrate preference that was reported earlier for purified NDM-1,[13,19] but the earlier values were collected using recombinant enzyme in which the metal content was not controlled or assessed for the enzyme in solution. Here, we find that the metal content of NDM-1 is variable under typical assay conditions, that these variations can result in significant changes to the rank order of substrate preference and to the rate constants for their hydrolysis, and that supplementation of zinc to presumably fill the M2 site results in maximal activity.

In summary, biochemical characterization of the major antibiotic resistance determinant of the NDM-1 superbug, New Delhi metallo-β-lactamase-1, shows that recombinant NDM-1 is released into the culture medium after N-terminal truncation, that this form of NDM-1 is monomeric, and that it is purified as a dizinc protein. However, the two zinc binding sites have different affinities, allowing the preparation of monozinc NDM-1, as well. Maximal activity for both monozinc NDM-1 and dizinc NDM-1 stocks after dilution into assay buffer is observed after supplementation with 10 μM zinc, but this effect is highly dependent on substrate structure, suggesting a dissimilar contribution of the second metal ion to catalysis of the hydrolysis of different classes of β-lactams. At optimal zinc concentrations, all β-lactam substrates tested were hydrolyzed by NDM-1, which displayed k_{cat}/K_M values as large as 10^7 M^{-1} s^{-1} and showed a slight preference for cephem substrates. This work provides a foundation for improving our understanding of the molecular basis for NDM-1-mediated antibiotic resistance and should allow more quantitative studies for the development of targeted therapeutics.

■ ASSOCIATED CONTENT

Ⓢ Supporting Information

NDM-1 coding sequence, substrate extinction coefficients, gel filtration studies, purification of NDM-1 from cytoplasmic extracts, and steady-state rate constants for dizinc and monozinc NDM-1 stocks supplemented with excess $ZnSO_4$. This material is available free of charge via the Internet at http://pubs.acs.org.

■ AUTHOR INFORMATION

Corresponding Author

*W.F.: College of Pharmacy, The University of Texas, PHARMED CHEM, 1 University Station, C0850, Austin, TX 78712; phone, (512) 232-4000; fax, (512) 232-2606; e-mail, WaltFast@mail.utexas.edu. D.X.: College of Chemistry, Sichuan University, Chengdu, Schuan 610064, China; e-mail, dgxu@scu.

edu.cn. D.L.: Department of Chemistry, Loyola University Chicago, 1032 W. Sheridan Rd., Chicago, IL 60660; e-mail, dliu@luc.edu.

Funding

This research was supported in part by a grant from the Robert A. Welch Foundation (F-1572 to W.F.). D.X. acknowledges support from the Natural Science Foundation of China (20803048, 21073125, and 31170675) and by the Program for New Century Excellent Talent in Universities (NCET-10-0606).

■ ABBREVIATIONS

NDM-1, New Delhi metallo-β-lactamase-1; EDTA, ethylenediaminetetraacetic acid; PDB, Protein Data Bank; MBL, metallo-β-lactamase; PCR, polymerase chain reaction; TEV, tobacco etch virus; PBS, phosphate-buffered saline; DTT, DL-dithiothreitol; TCEP, tris(2-carboxyethyl)phosphine hydrochloride; MD, molecular dynamics; QM/MM, quantum mechanical and molecular mechanical; SCC-DFTB, self-consistent charge density functional tight binding; VIM, verona integron-encoded metallo-β-lactamase; PAR, 4-(2-pyridylazo)-resorcinol; ESI-MS, electrospray ionization mass spectrometry; LMCT, ligand-to-metal charge transfer.

■ REFERENCES

(1) Fisher, J. F., Meroueh, S. O., and Mobashery, S. (2005) Bacterial resistance to β-lactam antibiotics: Compelling opportunism, compelling opportunity. *Chem. Rev. 105*, 395−424.

(2) Wang, Z., Fast, W., Valentine, A. M., and Benkovic, S. J. (1999) Metallo-β-lactamase: Structure and mechanism. *Curr. Opin. Chem. Biol. 3*, 614−622.

(3) Crowder, M. W., Spencer, J., and Vila, A. J. (2006) Metallo-β-lactamases: Novel weaponry for antibiotic resistance in bacteria. *Acc. Chem. Res. 39*, 721−728.

(4) Garau, G., Garcia-Saez, I., Bebrone, C., Anne, C., Mercuri, P., Galleni, M., Frere, J. M., and Dideberg, O. (2004) Update of the standard numbering scheme for class B β-lactamases. *Antimicrob. Agents Chemother. 48*, 2347−2349.

(5) Heinz, U., and Adolph, H. W. (2004) Metallo-β-lactamases: Two binding sites for one catalytic metal ion? *Cell. Mol. Life Sci. 61*, 2827−2839.

(6) Fitzgerald, P. M., Wu, J. K., and Toney, J. H. (1998) Unanticipated inhibition of the metallo-β-lactamase from *Bacteroides fragilis* by 4-morpholineethanesulfonic acid (MES): A crystallographic study at 1.85-Å resolution. *Biochemistry 37*, 6791−6800.

(7) Ullah, J. H., Walsh, T. R., Taylor, I. A., Emery, D. C., Verma, C. S., Gamblin, S. J., and Spencer, J. (1998) The crystal structure of the L1 metallo-β-lactamase from *Stenotrophomonas maltophilia* at 1.7 Å resolution. *J. Mol. Biol. 284*, 125−136.

(8) Bebrone, C., Delbruck, H., Kupper, M. B., Schlomer, P., Willmann, C., Frere, J. M., Fischer, R., Galleni, M., and Hoffmann, K. M. (2009) The structure of the dizinc subclass B2 metallo-β-lactamase CphA reveals that the second inhibitory zinc ion binds in the histidine site. *Antimicrob. Agents Chemother. 53*, 4464−4471.

(9) Huntley, J. J., Fast, W., Benkovic, S. J., Wright, P. E., and Dyson, H. J. (2003) Role of a solvent-exposed tryptophan in the recognition and binding of antibiotic substrates for a metallo-β-lactamase. *Protein Sci. 12*, 1368−1375.

(10) Merino, M., Perez-Llarena, F. J., Kerff, F., Poza, M., Mallo, S., Rumbo-Feal, S., Beceiro, A., Juan, C., Oliver, A., and Bou, G. (2010) Role of changes in the L3 loop of the active site in the evolution of enzymatic activity of VIM-type metallo-β-lactamases: Authors' response. *J. Antimicrob. Chemother. 65*, 1950−1954.

(11) Sabath, L. D., and Abraham, E. P. (1966) Zinc as a cofactor for cephalosporinase from *Bacillus cereus* 569. *Biochem. J. 98*, 11C−13C.

(12) Palmer, R. (2010) A disease—or gene—by any other name would cause a stink. *Nat. Med. 16*, 1059.

(13) Yong, D., Toleman, M. A., Giske, C. G., Cho, H. S., Sundman, K., Lee, K., and Walsh, T. R. (2009) Characterization of a new metallo-β-lactamase gene, bla(NDM-1), and a novel erythromycin esterase gene carried on a unique genetic structure in *Klebsiella pneumoniae* sequence type 14 from India. *Antimicrob. Agents Chemother. 53*, 5046−5054.

(14) Walsh, T. R. (2010) Emerging carbapenemases: A global perspective. *Int. J. Antimicrob. Agents 36* (Suppl. 3), S8−S14.

(15) Walsh, T. R., Weeks, J., Livermore, D. M., and Toleman, M. A. (2011) Dissemination of NDM-1 positive bacteria in the New Delhi environment and its implications for human health: An environmental point prevalence study. *Lancet Infect. Dis. 11*, 355−362.

(16) Guo, Y., Wang, J., Niu, G., Shui, W., Sun, Y., Zhou, H., Zhang, Y., Yang, C., Lou, Z., and Rao, Z. (2011) A structural view of the antibiotic degradation enzyme NDM-1 from a superbug. *Protein Cell 2*, 384−394.

(17) Zhang, H., and Hao, Q. (2011) Crystal structure of NDM-1 reveals a common β-lactam hydrolysis mechanism. *FASEB J. 25*, 2574−2582.

(18) King, D., and Strynadka, N. (2011) Crystal structure of New Delhi metallo-β-lactamase reveals molecular basis for antibiotic resistance. *Protein Sci. 20*, 1484−1491.

(19) Kim, Y., Tesar, C., Mire, J., Jedrzejczak, R., Binkowski, A., Babnigg, G., Sacchettini, J., and Joachimiak, A. (2011) Structure of Apo- and Monometalated Forms of NDM-1-A Highly Potent Carbapenem-Hydrolyzing Metallo-β-Lactamase. *PLoS One 6*, e24621.

(20) Thomas, P. W., Stone, E. M., Costello, A. L., Tierney, D. L., and Fast, W. (2005) The quorum-quenching lactonase from *Bacillus thuringiensis* is a metalloprotein. *Biochemistry 44*, 7559−7569.

(21) Thomas, P. W., and Fast, W. (2011) Heterologous overexpression, purification, and in vitro characterization of AHL lactonases. *Methods Mol. Biol. 692*, 275−290.

(22) Fast, W., Wang, Z., and Benkovic, S. J. (2001) Familial mutations and zinc stoichiometry determine the rate-limiting step of nitrocefin hydrolysis by metallo-β-lactamase from *Bacteroides fragilis*. *Biochemistry 40*, 1640−1650.

(23) Hunt, J. B., Neece, S. H., and Ginsburg, A. (1985) The use of 4-(2-pyridylazo)resorcinol in studies of zinc release from *Escherichia coli* aspartate transcarbamoylase. *Anal. Biochem. 146*, 150−157.

(24) Pollak, M., and Kuban, V. (1979) Comparison of Spectrophotometric Methods of Determination of Zinc(II) in Biological Material and Study of Its Complex Formation Reactions with 4-(2-Pyridylazo)resorcinol. *Collect. Czech. Chem. Commun. 44*, 725−741.

(25) Pace, C. N., Vajdos, F., Fee, L., Grimsley, G., and Gray, T. (1995) How to measure and predict the molar absorption coefficient of a protein. *Protein Sci. 4*, 2411−2423.

(26) Riccardi, D., Schaefer, P., Yang, Y., Yu, H., Ghosh, N., Prat-Resina, X., Konig, P., Li, G., Xu, D., Guo, H., Elstener, M., and Cui, Q. (2006) Development of effective quantum mechanical/molecular mechanical (QM/MM) methods for complex biological processes. *J. Phys. Chem. B 110*, 6458−6469.

(27) Elstner, M., Porezag, D., Jungnickel, G., Elsner, J., Haugk, M., Frauenheim, T., Suhai, S., and Seigert, G. (1998) Self-consistent-charge density-functional tight-binding method for simulations of complex materials properties. *Phys. Rev. B: Condens. Matter Mater. Phys. 58*, 7260−7268.

(28) Cui, Q., Elstner, M., Kaxiras, E., Frauenheim, T., and Karplus, M. (2001) A QM/MM implementation of the self consistent charge density functional tight binding (SCC-DFTB) method. *J. Phys. Chem. B 105*, 569−585.

(29) Elstner, M., Cui, Q., Munih, P., Kaxiras, E., Frauenheim, T., and Karplus, M. (2003) Modeling zinc in biomolecules with the self consistent charge density functional tight binding (SCC-DFTB) method: Applications to structure and energetic analysis. *J. Comput. Chem. 24*, 565−581.

(30) Wang, C., and Guo, H. (2007) Inhibitor binding by metallo-β-lactamase IMP-1 from *Pseudomonas aeruginosa*: Quantum mechanical/molecular mechanical simulations. *J. Phys. Chem. B 111*, 9986−9992.
(31) Xu, D., Guo, H., and Cui, Q. (2007) Antibiotic binding to dizinc β-lactamase L1 from *Stenotrophomonas maltophilia*: SCC-DFTB/CHARMM and DFT studies. *J. Phys. Chem. A 111*, 5630−5636.
(32) Xu, D., Guo, H., and Cui, Q. (2007) Antibiotic deactivation by dizinc β-lactamase: Mechanistic insights from QM/MM and DFT studies. *J. Am. Chem. Soc. 129*, 10814.
(33) Wu, S., Xu, D., and Guo, H. (2010) QM/MM studies of monozinc β-lactamase CphA suggest that the crystal structure of an enzyme-intermediate complex represents a minor pathway. *J. Am. Chem. Soc. 132*, 17986−17988.
(34) MacKerell, A. D. Jr., Bashford, D., Bellott, M., Dunbrack, R. L. Jr., Evanseck, J. D., Field, M. J., Fischer, S., Gao, J., Guo, H., Ha, S., Joseph-McCarthy, D., Kuchnir, L., Kuczera, K., Lau, F. T. K., Mattos, C., Michnick, S., Ngo, T., Nguyen, D. T., Prodhom, B., Reiher, W. E. III, Roux, B., Schlenkrich, M., Smith, J. C., Stote, R., Straub, J., Watanabe, M., Wiorkiewicz-Kuczera, J., Yin, D., and Karplus, M. (1998) All-atom empirical potential for molecular modeling and dynamics studies of proteins. *J. Phys. Chem. B 102*, 3586−3616.
(35) Field, M. J., Bash, P. A., and Karplus, M. (1990) A combined quantum mechanical and molecular mechanical potential for molecular dynamics simulations. *J. Comput. Chem. 11*, 700−733.
(36) Lassaux, P., Traore, D. A., Loisel, E., Favier, A., Docquier, J. D., Sohier, J. S., Laurent, C., Bebrone, C., Frere, J. M., Ferrer, J. L., and Galleni, M. (2011) Biochemical and structural characterization of the subclass B1 metallo-β-lactamase VIM-4. *Antimicrob. Agents Chemother. 55*, 1248−1255.
(37) Jorgensen, W. L., Chandrasekhar, J., Madura, J. D., Impey, R. W., and Klein, M. L. (1983) Comparison of simple potential functions for simulating liquid water. *J. Chem. Phys. 79*, 926−935.
(38) Brooks, C. L. III, Brunger, A., and Karplus, M. (1985) Active site dynamics in protein molecules: A stochastic boundary molecular-dynamics approach. *Biopolymers 24*, 843.
(39) Ryckaert, J. P., Ciccotti, G., and Berendsen, H. J. (1977) Numerical integration of the Cartesian equations of motion of a system with constraints: Molecular dynamics of n-alkanes. *J. Comput. Phys. 23*, 327−341.
(40) Daiyasu, H., Osaka, K., Ishino, Y., and Toh, H. (2001) Expansion of the zinc metallo-hydrolase family of the β-lactamase fold. *FEBS Lett. 503*, 1−6.
(41) Bebrone, C. (2007) Metallo-β-lactamases (classification, activity, genetic organization, structure, zinc coordination) and their superfamily. *Biochem. Pharmacol. 74*, 1686−1701.
(42) Aravind, L. (1999) An evolutionary classification of the metallo-β-lactamase fold proteins. *In Silico Biol. 1*, 69−91.
(43) Costello, A. L., Sharma, N. P., Yang, K. W., Crowder, M. W., and Tierney, D. L. (2006) X-ray absorption spectroscopy of the zinc-binding sites in the class B2 metallo-β-lactamase ImiS from *Aeromonas veronii bv. sobria*. *Biochemistry 45*, 13650−13658.
(44) Li, Y., Chooi, Y. H., Sheng, Y., Valentine, J. S., and Tang, Y. (2011) Comparative Characterization of Fungal Anthracenone and Naphthacenedione Biosynthetic Pathways Reveals an α-Hydroxylation-Dependent Claisen-like Cyclization Catalyzed by a Dimanganese Thioesterase. *J. Am. Chem. Soc. 133*, 15773−15785.
(45) Gomes, C. M., Giuffre, A., Forte, E., Vicente, J. B., Saraiva, L. M., Brunori, M., and Teixeira, M. (2002) A novel type of nitric-oxide reductase. *Escherichia coli* flavorubredoxin. *J. Biol. Chem. 277*, 25273−25276.
(46) Llarrull, L. I., Tioni, M. F., Kowalski, J., Bennett, B., and Vila, A. J. (2007) Evidence for a dinuclear active site in the metallo-β-lactamase BcII with substoichiometric Co(II). A new model for metal uptake. *J. Biol. Chem. 282*, 30586−30595.
(47) Carfi, A., Pares, S., Duee, E., Galleni, M., Duez, C., Frere, J. M., and Dideberg, O. (1995) The 3-D structure of a zinc metallo-β-lactamase from *Bacillus cereus* reveals a new type of protein fold. *EMBO J. 14*, 4914−4921.
(48) Orellano, E. G., Girardini, J. E., Cricco, J. A., Ceccarelli, E. A., and Vila, A. J. (1998) Spectroscopic characterization of a binuclear metal site in *Bacillus cereus* β-lactamase II. *Biochemistry 37*, 10173−10180.
(49) Davies, A. M., Rasia, R. M., Vila, A. J., Sutton, B. J., and Fabiane, S. M. (2005) Effect of pH on the active site of an Arg121Cys mutant of the metallo-β-lactamase from *Bacillus cereus*: Implications for the enzyme mechanism. *Biochemistry 44*, 4841−4849.
(50) Maret, W., and Vallee, B. L. (1993) Cobalt as probe and label of proteins. *Methods Enzymol. 226*, 52−71.
(51) Vallee, B. L., and Galdes, A. (1984) The metallobiochemistry of zinc enzymes. *Adv. Enzymol. Relat. Areas Mol. Biol. 56*, 283−430.
(52) Garmer, D. R., and Krauss, M. (1993) Ab initiio quantum chemical study of the cobalt d-d spectroscopy of several substituted zinc enzymes. *J. Am. Chem. Soc. 115*, 10247−10257.
(53) Lever, A. B. P. (1984) *Inorganic electronic spectroscopy*, 2nd ed., Elsevier, Amsterdam.
(54) Yamaguchi, Y., Ding, S., Murakami, E., Imamura, K., Fuchigami, S., Hashiguchi, R., Yutani, K., Mori, H., Suzuki, S., Arakawa, Y., and Kurosaki, H. (2011) A Demetallation Method for IMP-1 Metallo-β-lactamase with Restored Enzymatic Activity Upon Addition of Metal Ion(s). *ChemBioChem 12*, 1979−1983.
(55) Breece, R. M., Hu, Z., Bennett, B., Crowder, M. W., and Tierney, D. L. (2009) Motion of the zinc ions in catalysis by a dizinc metallo-β-lactamase. *J. Am. Chem. Soc. 131*, 11642−11643.
(56) Llarrull, L. I., Tioni, M. F., and Vila, A. J. (2008) Metal content and localization during turnover in *B. cereus* metallo-β-lactamase. *J. Am. Chem. Soc. 130*, 15842−15851.